Estimation of multifractality based on natural time analysis

Mintzelas, A., Sarlis, N. V. & Christopoulos, S.

DOI 10.1016/j.physa.2018.08.015
ISSN 0378-4371

Publisher: Elsevier

Estimation of multifractality based on natural time analysis

A. Mintzelas,[1,*] N. V. Sarlis,[1,2,†] and S.-R. G. Christopoulos[3,2,‡]

[1]*Section of Solid State Physics, Department of Physics, School of Science, National and Kapodistrian University of Athens, Panepistimiopolis, Zografos 157 84, Athens, Greece*

[2]*Solid Earth Physics Institute, Department of Physics, School of Science, National and Kapodistrian University of Athens, Panepistimiopolis, Zografos 157 84, Athens, Greece*

[3]*Faculty of Engineering, Environment and Computing, Coventry University, Priory Street, Coventry CV1 5FB, United Kingdom*

Abstract

Recent studies have shown that results deduced on the basis of a new time domain termed natural time reveal that novel dynamical features hidden behind time-series in complex systems can be uncovered. Here, we propose a method for estimating the multifractal behavior of time series by studing the fluctuations of natural time under time reversal. Examples of the application of this method to fractional Gaussian noises, fractional Brownian motions, binomial multifractal series, Lévy processes as well as interbeat intervals' time series from electrocardiograms are presented.

PACS numbers: 05.45.Tp, 05.40.-a, 89.75.-k, 64.60.al, 87.10.-e, 87.19.Hh

Keywords: time reversal, natural time, multifractals, fGn, fBm, heart rate variability

*Electronic address: a.mintzelas@gmail.com

†Electronic address: nsarlis@phys.uoa.gr

‡Electronic address: ac0966@coventry.ac.uk

I. INTRODUCTION

In most cases, the time-series resulting from physical systems and processes exhibit correlations that decay exponentially. However, it is well known[1, 2] that a major exception is when approaching a critical point, the exponential decay turns into a power-law decay. Moreover, long range power-law correlations have been found in a wide variety of systems including complex systems, e.g., see Ref.[3]. Such systems give rise to time-series that exhibit scale-invariant features characterized by long-range power law correlations. Since their superposition with erratic fluctuations due to, for example, noise in the emitted signals, may be unavoidable or the amount of experimental data may be small, it is very important to investigate techniques that may identify such long-range power law correlations. This is main the scope of the present paper by employing the new time domain termed natural time [4–8] which may uncover hidden properties in the time-series of complex systems.

In general, a stochastic process $X(t)$ is called [9, 10] self-similar with index H if it has the property $X(\lambda t) \stackrel{d}{=} \lambda^H X(t)$, where $\stackrel{d}{=}$ denotes the usual equality of finite-dimensional distributions. Such a process generates time series which is characterized by an unique scaling exponent H in their entire length. This kind of time series is called monofractal time series [11].

In reality, the majority of time series does not exhibit a simple monofractal scaling behavior, which can be accounted for by a single scaling exponent H. As mentioned in Ref. [12], there is the possibility of crossover (time-) scales s_x separating regimes with different scaling exponents [13, 14], e. g. long-range correlations on small scales s ($s << s_x$) and another type of correlations or uncorrelated behavior on larger scales s ($s >> s_x$). In other cases, the scaling behavior is more complicated, and different scaling exponents are required for different parts of the series [15]. Such time series, where more than one scaling exponent (set of scaling exponents) is needed in order to describe their scaling properties are called multifractal time series, e.g., [16–25].

Detrended Fluctuation Analysis (DFA) constitutes a well-established method for the determination of the scaling exponent H in monofractal time series [26, 27] as well as its generalization Multifractal Detrended Fluctuation Analysis (MFDFA) in the case of multifractal time series [12]. Another widely adopted [28] method for estimating the multifractal behavior in non-stationary observational records, is the wavelet transform modulus max-

ima (WTMM) method [29, 30] which involves, however, a more complicated mathematical treatment. WTMM has been compared [12, 31, 32] to MFDFA and the results show [33] that MFDFA is at least equivalent to WTMM, while the latter needs more care and may yield spurious multifractality [32]. An alternative multifractal method that has [33] even less computational difficulties than MFDFA, is the one based on the Centered Moving Average (CMA) technique [34, 35], that improves the classical causal backward moving average method [36, 37] (see also [38]), and is called multifractal CMA (MFCMA). Since CMA performs better than DFA in the limit of very small and very large scales, MFCMA is more suitable [33] for short time series. Of course, the detrending made in MFCMA is not as strong as in MFDFA, thus one may consider MFCMA for data without significant trends and MFDFA for data with intense trends [33], like polynomials of large curvature or periodicities of high amplitude and/or frequency. Natural time [4–8] and more specifically the fluctuations of its average value under time reversal, can also capture [39] the scaling properties of a monofractal time series by means of the determination of its scaling exponent H. Here, we attempt a generalization of this method to the multifractal case.

In Sec. II, we describe the basics of natural time analysis including the fluctuations of the average value of natural time under time reversal and introduce the Generalized Fluctuations of the average value of Natural Time under time reversal (GFNT). In the same Section, we present the methodology we adopt to estimate the set of generalized scaling exponent $h(q)$ of a mulltifractal time series and its singularity spectrum $f(\alpha)$. Furthermore, in Sec. III, we examine various time series, comparing the results coming from the different methods: MFDFA, MFCMA and GFNT. Finally, Sec. IV summarizes our conclusions.

II. METHODOLOGY

A. Natural Time Analysis

In a time series comprising N events, the natural time $\chi_k = k/N$ serves as an index for the occurrence of the k-th event [4, 5]. In natural time analysis the evolution of the pair (χ_k, Q_k) is considered, where Q_k denotes in general a quantity proportional to the energy released in the k-th event. For example, for dichotomous signals, Q_k stands for the duration of the k-th pulse while for the seismicity Q_k is proportional to the seismic

energy released during kth earthquake [6, 40–47]. Usually instead of Q_k, the normalized energy release $p_k = Q_k / \sum_{i=1}^{N} Q_i$ is used [7]. The latter sum up to unity, $\sum_{k=1}^{N} p_k = 1$, and can be considered as probability [48] giving rise to an average value of natural time $\langle \chi \rangle = \sum_{k=1}^{N} \chi_k p_k$. This value changes [39] if we consider the action [49–51] of the time-reversal $\hat{T} p_k = p_{N-k+1}$ that makes the first pulse to be considered as the last one, the second as the last but one etc.

It is noteworthy that the physical meaning of the difference of average value of natural time χ under time reversal, i.e., of the quantity $\langle \chi \rangle - \langle \hat{T} \chi \rangle$, can be revealed if we consider the parametric family of the distributions $p(\chi; \epsilon) = 1 + \epsilon(\chi - 1/2)$. For small ϵ ($\ll 1/2$), these distributions correspond to small trends superimposed on a uniform distribution [22, 52]. Direct calculation of $\langle \chi \rangle \equiv \int_0^1 \chi p(\chi; \epsilon) \mathrm{d}\chi$ yields $\langle \chi \rangle = 1/2 + \epsilon/12$ and since $\hat{T} p(\chi; \epsilon) = p(\chi; -\epsilon)$, one obtains that $\langle \chi \rangle - \langle \hat{T} \chi \rangle = \epsilon/6$. Thus, the average value of natural time under time reversal is proportional to the 'local' trend ϵ and the study of its fluctuations, which is the subject of the next subsection, is actually the study of how these 'local' trends fluctuate in a time-series.

1. *Fluctuations of the average value of natural time under time reversal.*

In order to study the long-range dependence in a time series, e.g., $Q_k, \{k = 1, 2, \ldots, N\}$, we have to define a scale-dependent measure (for example, the detrended fluctuation $F_d(l)$ constitutes [26] such a measure in DFA). Natural time and particularly the fluctuations of natural time under time reversal, may constitute [39] such a scale-dependent measure enabling us to introduce a reliable method to extract the scaling exponent H of a monofractal time series.

The fluctuation of the average value of natural time under time reversal within scale l is

$$\Delta\chi_l = \sqrt{E[(\langle \chi \rangle - \langle \widehat{T} \chi \rangle)^2]} \tag{1}$$

Considering a sliding window of length l starting from Q_{m_0} (thus ending at Q_{m_0+l-1}), the values of natural time are given by $\chi_k = k/l$ for $k = 1, 2, ..., l$ and correspond to the point probabilities $p_k = Q_{m_0+k-1} / \sum_{i=1}^{l} Q_{m_0+i-1}$. Since under time reversal, we have $\hat{T} p_k = p_{l-k+1}$,

Eq.(1) can be alternatively written as

$$\Delta\chi_l^2 = E\left\{ \left[\sum_{k=1}^{l} \frac{k}{l}(p_k - p_{l-k+1}) \right]^2 \right\} \tag{2}$$

where the symbol $E[...]$ denotes the expectation value obtained when a window of length l is sliding through the time series Q_k. The evaluation of $E[...]$ is carried out by full computation. By expanding the square in the right hand side of Eq. (2), we obtain

$$\Delta\chi_l^2 = \sum_{k=1}^{l} \left(\frac{k}{l}\right)^2 E[(p_k - p_{l-k+1})^2] + \sum_{k\neq m} \frac{km}{l^2} E[(p_k - p_{l-k+1})(p_m - p_{l-m+1})] \tag{3}$$

The quantities p_k as mentioned sum up to unity, i.e., $\sum_{k=1}^{l} p_k = 1$ or equivalently $p_k = 1 - \sum_{m\neq k} p_m$. By subtracting from the last expression its value for $k = l - k + 1$, we obtain $p_k - p_{l-k+1} = -\sum_{m\neq k} p_m - p_{l-m+1}$, and hence

$$(p_k - p_{l-k+1})^2 = -\sum_{m\neq k} (p_k - p_{l-k+1})(p_m - p_{l-m+1}) \tag{4}$$

By substituting Eq. (3) into Eq. (4), we obtain

$$\Delta\chi_l^2 = -\sum_{k=1}^{l} \left(\frac{k}{l}\right)^2 \sum_{m\neq k} E[(p_k - p_{l-k+1})(p_m - p_{l-m+1})] + \sum_{k\neq m} \frac{km}{l^2} E[(p_k - p_{l-k+1})(p_m - p_{l-m+1})] \tag{5}$$

which simplifies to

$$\Delta\chi_l^2 = -\sum_{k,m} \frac{(k-m)^2}{l^2} E[(p_k - p_{l-k+1})(p_m - p_{l-m+1})] \tag{6}$$

The negative sign appears because $(p_k - p_{l-k+1})$ and $(p_m - p_{l-m+1})$ are in general anticorrelated due to Eq. (4). Equation (6) implies that $\Delta\chi_l^2$ measures the long-range correlations in Q_k. If we assume that $-E[(p_k - p_{l-k+1})(p_m - p_{l-m+1})] \propto (k-m)^{2\chi_H}/l^2$ (cf. p_k scales as $1/l$ due to the condition $\sum_{k=1}^{l} p_k = 1$, e.g., see [53]), we have that

$$\Delta\chi_l^2 \propto \frac{l^{4+2\chi_H}}{l^4} \tag{7}$$

so that

$$\Delta\chi_l(\equiv\sqrt{\Delta\chi_l^2})\propto l^{\chi_H} \tag{8}$$

where χ_H is a scaling exponent. Obviously, we can calculate it from the slope of the graph $\log(\Delta\chi_l)$ versus $\log(l)$. As it was shown [39], in the case of fractional Brownian motion(fBm) the scaling exponent χ_H is identical to the corresponding scaling exponent H

$$H=\chi_H \tag{9}$$

while in case of fractional Gaussian noise (fGn) the following condition holds

$$H=1+\chi_H. \tag{10}$$

2. Generalized fluctuations of the average value of natural time under time reversal.

We observe that Eq. (1) involves a second order moment in analogy to the relation that governs DFA [26, 27, 54]. With a similar thinking that led from DFA to MFDFA [12], we define the $q-th$ order variance of natural time under time reversal through the equation

$$\Delta\chi_l(q)=\Big(E[((\langle\chi\rangle-\langle\widehat{T}\chi\rangle)^2)^{q/2}]\Big)^{1/q} \tag{11}$$

which when it scales as

$$\Delta\chi_l(q)\sim l^{\chi_H(q)} \tag{12}$$

it may lead to the exponents $\chi_H(q)$. As a strict analogy to DFA and MFDFA, we notice that in the case of $q=2$ the generalized fluctuations of natural time under time reversal (GFNT) revert to ordinary fluctuations of the average value of natural time under time reversal.

B. Procedure to compare GFNT with MFDFA or MFCMA

In order to examine the ability of GFNT, i.e., Eq. (12), to capture the multifractal scaling properties through $\chi_H(q)$ and compare its performance to MFDFA or MFCMA, the following procedure is adopted:

1. We generate monofractal and multifractal time series X_k, with generalized scaling exponents which are analytically calculated or known in advance.

2. We calculate the sets of generalized scaling exponents $h(q)$ with the help of MFDFA as described in Appendix A or by following MFCMA as described in Appendix B. In both cases, the original time series X_k is used for both analyses.

3. In natural time analysis Q_k should be positive. So, we normalize the resulting X_k time series to zero mean and unit standard deviation and then add to the normalized time series N_k twice the minimum of N_k to ensure the positivity of $Q_k = N_k + 2|\min(N_k)|$.

4. We calculate the scaling exponents $\chi_H(q)$ with the help of generalized fluctuations of natural time under time reversal, i.e., Eqs. (11) and (12), by fitting in a wide range of scales l. We have empirically observed that the GFNT performance may improve if an additional summation step is adopted. In such cases, we determine the profile using the summation process defined by the equation

$$y(i) = \sum_{k=1}^{i} (X_k - \bar{X}) \tag{13}$$

where $y(i)$ is the profile and $\bar{X}$ the mean value given by

$$\bar{X} = \frac{1}{N} \sum_{i=1}^{N} X_i. \tag{14}$$

We then repeat the third step by considering the profile $y(i)$ as X_k to ensure positivity of Q_k and calculate $\chi_H(q)$.

5. For further analysis, we may calculate the corresponding singularity spectrum [55] $f(\alpha)$. Following Kantelhardt et al. [12], we first determine the global scaling exponent $\tau(q)$ from the relation

$$\tau(q) = qH(q) - 1 \tag{15}$$

where $H(q)$ is the generalized scaling exponent, i.e., $h(q)$ of MFDFA and MFCMA or $\chi_H(q)$ of GFNT, and q is the order of the fluctuation. Second, we define as usual [55] the singularity spectrum $f(\alpha)$, using $H(q)$ with the help of Legendre transformation [56]

$$f(\alpha) = \alpha q - \tau(q) \tag{16}$$

where

$$\alpha = \alpha(q) \equiv \frac{\partial \tau(q)}{\partial q}. \tag{17}$$

For the time series studied in subsection III D, the evaluation of the parameter α in Eq. (17) is made by using three-point differentiation since there is no analytical form for the global exponent $\tau(q)$. For a more detailed and accurate view of the width of the singularity spectrum, we fit a second order polynomial to these points, generating a parabolic function which corresponds to the singularity spectrum. The α value assigned to the maximum of this second order polynomial, labeled α_{max}, as well as the distance $|\alpha' - \alpha''|$ between the two α-values that correspond to the same pre-defined $f(\alpha)$-value, e.g. $f(\alpha') = f(\alpha'') = 0.75$, are of great importance for our analysis (e.g., see Fig.5(c) that will be discussed latter in subsection III D).

III. APPLICATIONS

A. Fractional Brownian motion

Fractional Brownian motion (fBm) introduced by Mandelbrot and van Ness [57] has already found many physical applications (e.g., see Refs. [58, 59]). As a first example, we generate 3×10^2 monofractal fBm time series X_k (consisting of 10^4 points) for a given value of the scaling exponent H using the Mandelbrot-Weierstrass function [49, 60, 61] and analyze them with the help of the generalized fluctuations of natural time under time reversal by fitting in the range of scales $4 \leq l \leq 10^3$. The values obtained for $\chi_H(q)$ are used for the construction of the statistics depicted in Fig. 1. The distribution of the multifractal spectra obtained in each case are depicted in this figure by the mean value of $\chi_H(q)$ (blue solid circles) and the corresponding standard deviation (cf. the mean value of their estimation error is very close to the depicted standard deviation).

In order to compare these GFNT results with other multifractal methods, we used a computer code named `mfdfa.c` implementing MFDFA [12] kindly provided to us by Professor Doctor Jan Kantelhardt and used a fitting range of $s = 10 - 2400$. The corresponding results for the average values of $h(q) - 1$ are shown by the green squares while the green shaded region indicates the one standard deviation interval. Additionally, MFCMA (see Appendix B) has been also applied using a fitting range of $s = 10 - 2400$ and the results are shown in

Fig.1 by the inverted red triangles (mean values) and the red shaded region (± one standard deviation).

Although we expect that the estimated generalized scaling exponents $\chi_H(q)$ of GFNT should be independent from q, the results shown in Fig. 1 exhibit a deviation from the expected H value. One can observe that GFNT exhibits stability for negative values of q, however, with much larger error when comparing with MFDFA. For the positive values of q, the GFNT is approaching the MFDFA in the cases of $H = 0.3, H = 0.5, H = 0.7$ especially within the range of $0 \leq q \leq 6$. Also, the results of GFNT and MFDFA for positive q tend to be closer for small values of H. When studying the results obtained from MFCMA, we observe an even smaller variation of $h(q)$. MFCMA performs better than the other methods for positive q, in accordance with the suggestion of Ref.[33], but for negative q GFNT gives a more stable result at the expense, however, of a larger standard deviation. In summary, the scaling exponents $\chi_H(q)$ for the majority of the H values studied have an almost comparable behavior with those of MFDFA or MFCMA for these monofractal time series.

B. Binomial multifractal series

In the binomial multifractal model, a series of $N = 2^{n_{max}}$ numbers with $k = 1, ..., N$ is defined by

$$x_k = \alpha^{n(k-1)}(1-\alpha)^{n_{max}-n(k-1)} \tag{18}$$

where $0.5 < \alpha < 1$ is a parameter and $n(k)$ is the number of digits equal to 1 in the binary representation of the number k (for instance $n(13) = 3$, since 13 corresponds to binary 1101). The generalized Hurst exponent $h(q)$ can be analytically evaluated (e.g., see Ref. [12]) leading to the expression

$$h(q) = \frac{1}{q} - \frac{\ln[\alpha^q + (1-\alpha)^q]}{q \ln(2)}. \tag{19}$$

We generated such time series consisting of 8192 points ($n_{max} = 13$ with $\alpha = 0.7, 0.8, 0.9$ and estimated the generalized scaling exponents by MFDFA method (see the green squares and the corresponding green region in Fig. 2).

As far as GFNT method is concerned, binomial time series constitute a representative example where the aforementioned additional step of summation is required. Subsequently, we generate and analyze the profile (instead of original time series) in natural time by evaluating scaling exponents $\chi_H(q)$ (fig. 2). More specifically, for the positive q-values we use for calculation the range $l = 8-158$ and for the negative q-values the range $l = 50-1000$.

Thus, we proceed to the comparison of the generalized scaling exponents $h(q)$ calculated by MFDFA (green color) (using `mfdfa.c` and fitting in the range 50-1000) and $\chi_H(q)$ by GFNT (blue color) versus the theoretical set of generalized scaling exponents $h(q)$ for binomial multifractal time series for three different values of α, for $\alpha = 0.7, 0.8$ and 0.9. For the negative q values, the results show that the GFNT estimators are equal or better than those obtained by MFDFA. For the positive q values, the results show that the GFNT estimators are much better than those obtained by MFDFA and extremely close to the corresponding theoretical values. This conclusion is not altered if we also consider the additional results obtained by employing MFCMA (fitting in the range 50-1000), which are shown in Fig.2 with the cyan inverted triangles.

Having the scaling exponents $\chi_H(q)$ from GFNT, we calculate the singularity spectra for the three cases $\alpha = 0.7, 0.8$ and 0.9 as shown in Fig.3 and compare them with those theoretically obtained. The observed convergence of the points strengthens the validation of the GFNT method.

C. Lévy processes

Uncorrelated process obeying a distribution with an asymptotic power law behavior, $P(x) \sim x^{-(\alpha_L+1)}$, for large x, will have infinite variance if $0 < \alpha_L \leq 2$ [23]. Here, we examine a typical example of such a process which is the stable Lévy process.

More specifically we calculate the generalized scaling exponents (with MFDFA, MFCMA and GFNT) of a time series (consisting of 262144 points) which obeys power law with exponent $\alpha_L + 1 = 2.5$. The time series is coming from Ref. [23] and is available online at `http://lps.lncc.br/index.php/demonstracoes/emd-damf`. It has a well-known set of generalized scaling exponents [62]:

$$h(q) = \begin{cases} 1/\alpha_L & q \leq \alpha_L \\ 1/q & q > \alpha_L \end{cases} \tag{20}$$

Our results are shown in Fig.4 where the range of l =5 to 2511 has been used in GFNT. We observe that the generalized scaling exponents $\chi_H(q)$ which are calculated by GFNT are closer to the theoretical curve than those obtained by MFDFA (when using `mfdfa.c` and fitting in the aforementioned range of 5 to 2511). Additional results obtained by fitting in the same range and using MFCMA (depicted in Fig.4 by the cyan inverted triangles) differ from the theoretical curve on average as much as those of GFNT. MFCMA, however, exhibits an average value of $h(q)$ for negative q which is slightly closer to the theortical one than that of GFNT.

D. Application to heart variability data

Apart from the synthetic multifractal time series used so far, here we analyze heart rate variability data which are well known [19, 24, 63–67] to exhibit multifractal properties as well. These data come from 134 long-lasting (from several hours to around 24 h) electrocardiograms (ECG) of Physionet [68] available from `https://physionet.org/`. These contain: (i) 72 healthy subjects which will be labeled H and come from the MIT-BIH Normal Sinus Rhythm Database (nsrdb) containing 18 H and the Normal Sinus Rhythm RR Interval Database (nsr2db) containing 54 H (with sampling frequency f_{exp}=128Hz), (ii) 44 patients suffering from congestive heart failure (CHF) coming from the CHF RR Interval Database (chf2db) containing 29 subjects with f_{exp}=128Hz and the BIDMC CHF Database (chfdb) with 15 subjects with severe CHF which is a subset of the data described in Ref. [69] (f_{exp}=250Hz), and (iii) the Sudden Cardiac Death Holter Database (sddb) with f_{exp}=250Hz. The latter database contains 24 records among which 12 were ECG with audited annotations. Beyond these 12 cases, we also study six more (i.e., '33', '37', '44', '47', '48', '50') that could be analyzed with confidence [50].

The time series that were analyzed by GFNT are those corresponding to the NN intervals, i.e., X_k=NN$_k$, $k = 1, 2, \ldots N$ (cf. these intervals are obtained [70] from the ECG annotation files by using the option '-c -PN -pN', which yields only intervals between consecutive normal beats and intervals between pairs of normal beats surrounding an ectopic beat are discarded

from the output). Additionally, following Ref. [19], we eliminated the outliers due to missed beat detections that may give rise to large intervals included in the NN time series. For each of the 134 NN time series $\chi_H(q)$ was estimated for scales l in the range 5 to $\approx N/4$, where N is the total number of NN intervals in the time series and typical examples are shown in Fig.5(a). Here, we note that since we analyze interval time series from ECGs that have been digitized with different sampling rates we focus on the region of positive q-values since the small fluctuations enhanced by negative q's are expected to be significantly affected by digitization. According to the procedure described above in subsection II B, we constructed $\tau(q)$, see Fig.5(b), and from a three-point differentiation we obtained the spectra shown in Fig.5(c). As it has been established [11, 19, 71–74], the multifractal properties of the heart beat intervals time series convey useful information concerning a well-functioning healthy heart.

In view of this fact, we quantify here the multifractal spectrum by means of the quantities α_{max}, i.e., the value of α at which the parabolic approximation used maximizes, and $|\alpha' - \alpha''|$, which is the width of the parabolic spectrum at $f(\alpha') = f(\alpha'') = 0.75$, that were defined in subsection II B. Figure 6 depicts α_{max} versus $|\alpha' - \alpha''|$ for all the 134 time series analyzed. A quick look at this figure reveals that the points corresponding to healthy individuals fall, as expected, within a well-defined region bounded by the cyan ellipse of Fig.6 . Apart from the 72 healthy, this ellipse encloses only 6 (out of 18) SCD and more interestingly only 2 (out of 15) New York Heart Association (NYHA) class IV CHF patients. For CHF patients of NYHA classes III and II only 36% fall outside the cyan ellipse, whereas for NYHA class I only 1 (out of 4) does so. Finally, it is worthwhile to mention that the separation between different heart patients based on Fig.6 can be considered as complementary to other methods suggested on the basis of natural time for the same reason. For example, the case of the SCD individual labeled '47' mixes with H in Fig.5 of Ref. [51] while in Fig.6 the corresponding point lies well outside the cyan ellipse of the healthy. Moreover, a comparison with the data depicted in Fig.5 of Ref. [51] with Fig.6 reveals that only one ('chf12') NYHA class IV CHF patient mixes with the healthy.

IV. CONCLUSIONS

Generalizing the fluctuations of natural time under time reversal in a way similar to the transition from DFA to MFDFA, we constructed a method named GFNT based on an exponent $\chi_H(q)$ which can capture the scaling properties of multifractal time series. As it has been shown by the applications presented here, the generalized scaling exponents $\chi_H(q)$ are very close to the theoretically expected values as well as to those found by MFDFA and MFCMA . For negative q values, GFNT may be more accurate though less precise than MFDFA. Finally, GFNT has been also applied to NN interval time series obtained from ECG recordings. The results exhibit a robust behavior for the healthy group that allows the separation of 13 (out 15) NYHA class IV CHF patients.

Acknowledgments

The authors would like to express their sincere thanks to Professor Doctor Jan Kantelhardt for various constructive suggestions on the manuscript as well as for providing his computer code implementing MFDFA.

APPENDIX A: BRIEF DESCRIPTION OF MFDFA

The multifractal detrended fluctuation analysis usually abbreviated MFDFA constitutes the generalization of DFA [26, 27]. MFDFA methodology consists of five steps [12]. Supposing that we have a time series X_k comprising of N points:

1. Firstly, we calculate the 'profile' time series $y(i) = \sum_{k=1}^{i}(X_k - \bar{X})$ where $\bar{X} = \sum_{k=1}^{N} X_k/N$.

2. As a second step, we divide the profile time series in N_s non-overlapping segments of equal length s, $N_s = N/s$.

3. Then, we calculate the trend for each segment s via the methodology of least-square fit by using a polynomial of order n and determine the variance

$$F^2(s,v) = \frac{1}{s}\sum_{i=1}^{s}\Big\{y[(v-1)s+i] - y_v(i)\Big\}^2 \tag{A1}$$

where $y_v(i)$ is the fitting polynomial at the i-th point of the v-th non-overlapping segment.

4. Averaging over all segments results in the q-th order fluctuation function

$$F_q(s) = \left\{ \frac{1}{N_s} \sum_{v=1}^{N_s} F^2(s,v)^{q/2} \right\}^{1/q} \tag{A2}$$

where the index variable q can be assigned with any real value except zero. For $q = 2$, DFA is retrieved.

5. Finally, for the determination of the scaling behavior of time series, we analyze log-log plots of $F_q(s)$ versus s for each value of q to end up at the set of generalized scaling exponents $h(q)$ according to

$$F_q(s) \propto s^{h(q)}. \tag{A3}$$

Due to the summation in step 1, we have to subtract unity from $h(q)$ in order to compare with $\chi_H(q)$, when the original analyzed time-series X_k is used for GFNT.

APPENDIX B: BRIEF DESCRIPTION OF MFCMA

The multifractal centered moving average analysis usually abbreviateed MFCMA consists [33] of the following steps. Supposing that we have a time series X_k comprising of N points:

1. Firstly, we calculate the 'profile' time series $y(i) = \sum_{k=1}^{i}(X_k - \bar{X})$ where $\bar{X} = \sum_{k=1}^{N} X_k/N$.

2. As a second step, a centered moving average of an odd window length s is obtained for every point i of the profile $y(i)$

$$\mathrm{CMA}_s(i) = \frac{1}{s} \sum_{j=-[s/2]}^{[s/2]} y(i+j), \tag{B1}$$

where $[s/2]$ is the integer part of $s/2$ which is $[s/2] = (s-1)/2$ since s is odd. For indices i at the edges of the profile (e.g. for $i \geq 1$ and $i \leq [s/2]$) the centered moving

average does not exist. One may ignore these points, or (which the case used in the present manuscript) use a cyclic continuation of the time series by connecting the very last part of the profile to the beginning by assuming $y(0) = 0$.

3. As a third step, the profile time series is divided in $2[N/s]$ non-overlapping windows ν of equal length s. For each window $\nu = 0, \ldots, [N/s] - 1$ the fluctuation of the profile around the centered moving average (in the forward direction) is given by

$$F^2_{\mathrm{CMA},\nu}(s) = \frac{1}{s}\sum_{i=1}^{s}[y(\nu s + i) - \mathrm{CMA}_s(\nu s + i)]^2, \tag{B2}$$

whereas for the backward direction and $\nu = [N/s], \ldots, 2[N/s] - 1$

$$F^2_{\mathrm{CMA},\nu}(s) = \frac{1}{s}\sum_{i=1}^{s}\left\{y\left[N - (\nu - [N/s] + 1)s + i\right] - \mathrm{CMA}_s\left[N - (\nu - [N/s] + 1)s + i\right]\right\}^2. \tag{B3}$$

4. Then, the fluctuation measure of MFCMA is defined as

$$F_{\mathrm{MFCMA},q}(s) = \left\{\frac{1}{2[N/s]}\sum_{\nu=0}^{2[N/s]-1}[F^2_{\mathrm{CMA},\nu}(s)]^{q/2}\right\}^2 \tag{B4}$$

5. Ideally, $F_{\mathrm{MFCMA},q}(s)$ follows a power law for a certain range of scales s,

$$F_{\mathrm{MFCMA},q}(s) \propto s^{h(q)}, \tag{B5}$$

and the generalized exponent $h(q)$ can be determined by straight line fits in the log-log plots of $F_{\mathrm{MFCMA,q}}(s)$ versus s. Due to the summation in step 1, we have to subtract unity from $h(q)$ in order to compare with $\chi_H(q)$. For the case of fBm studied in subsection III A and in order to minimize summation errors, we employed the above procedure for the fBm increments, i.e., the corresponding fractional Gaussian noise. Obviously, in this case $h(q)$ can be directly compared with $\chi_H(q)$.

---

[1] H. E. Stanley, Nature **378**, 554 (1995).

[2] H. E. Stanley, Rev. Mod. Phys. **71**, S358 (1999).

[3] D. Sornette, in *Encyclopedia of Complexity and Systems Science*, edited by R. A. Meyers (Springer New York, New York, NY, 2009), pp. 7009–7024.

[4] P. A. Varotsos, N. V. Sarlis, and E. S. Skordas, Practica of Athens Academy **76**, 294 (2001).

[5] P. A. Varotsos, N. V. Sarlis, and E. S. Skordas, Phys. Rev. E **66**, 011902 (2002).

[6] P. A. Varotsos, N. V. Sarlis, and E. S. Skordas, Acta Geophysica Polonica **50**, 337 (2002).

[7] P. A. Varotsos, N. V. Sarlis, and E. S. Skordas, *Natural Time Analysis: The new view of time. Precursory Seismic Electric Signals, Earthquakes and other Complex Time-Series* (Springer-Verlag, Berlin Heidelberg, 2011).

[8] P. Varotsos, N. V. Sarlis, E. S. Skordas, S. Uyeda, and M. Kamogawa, Proc. Natl. Acad. Sci. USA **108**, 11361 (2011).

[9] J. W. Lamperti, Trans. Am. Math. Soc. **104**, 62 (1962).

[10] B. Mandelbrot, Science **156**, 636 (1967).

[11] H. Stanley, L. Amaral, A. Goldberger, S. Havlin, P. Ivanov, and C.-K. Peng, Physica A **270**, 309 (1999).

[12] J. Kantelhardt, S. A. Zschiegner, E. Koscienly-Bunde, A. Bunde, S. Havlin, and H. E. Stanley, Physica A **316**, 87 (2002).

[13] J. W. Kantelhardt, E. Koscielny-Bunde, H. H. A. Rego, S. Havlin, and A. Bunde, Physica A **295**, 441 (2001).

[14] K. Hu, P. C. Ivanov, Z. Chen, P. Carpena, and H. E. Stanley, Phys. Rev. E **64**, 011114 (2001).

[15] Z. Chen, P. C. Ivanov, K. Hu, and H. E. Stanley, Phys. Rev. E **65**, 041107 (2002).

[16] C. Meneveau and K. R. Sreenivasan, Phys. Rev. Lett. **59**, 1424 (1987).

[17] R. Pastor-Satorras, Phys. Rev. E **56**, 5284 (1997).

[18] B. B. Mandelbrot, *Multifractals and 1/f Noise* (Springer-Verlag, New York, 1999).

[19] P. C. Ivanov, M. G. Rosenblum, C.-K. Peng, J. Mietus, S. Havlin, H. E. Stanley, and A. L. Goldberger, Nature **399**, 461 (1999).

[20] P. C. Ivanov, L. A. N. Amaral, A. L. Goldberger, S. Havlin, M. G. Rosenblum, H. E. Stanley, and Z. R. Struzik, Chaos **11**, 641 (2001).

[21] L. Telesca, V. Lapenna, and F. Vallianatos, Phys. Earth Planet. Int. **131**, 63 (2002).

[22] P. A. Varotsos, N. V. Sarlis, and E. S. Skordas, Phys. Rev. E **67**, 021109 (2003).

[23] G. S. Welter and P. A. Esquef, Physical Review E **87**, 032916 (2013).

[24] P. C. Ivanov, Z. Chen, K. Hu, and H. E. Stanley, Physica A **344**, 685 (2004).

[25] L. Telesca, A. Chamoli, M. Lovallo, and T. Stabile, Pure Appl. Geophys. pp. 1–11 (2014).

[26] C.-K. Peng, S. V. Buldyrev, S. Havlin, M. Simons, H. E. Stanley, and A. L. Goldberger, Phys. Rev. E **49**, 1685 (1994).

[27] C. K. Peng, S. V. Buldyrev, A. L. Goldberger, S. Havlin, R. N. Mantegna, M. Simons, and H. E. Stanley, Physica A **221**, 180 (1995).

[28] J. Ludescher, M. I. Bogachev, J. W. Kantelhardt, A. Y. Schumann, and A. Bunde, Physica A **390**, 2480 (2011).

[29] J. F. Muzy, E. Bacry, and A. Arneodo, Phys. Rev. Lett. **67**, 3515 (1991).

[30] J. F. Muzy, E. Bacry, and A. Arneodo, Int. J. Bifurcation Chaos **4**, 245 (1994).

[31] J. W. Kantelhardt, D. Rybski, S. A. Zschiegner, P. Braun, E. Koscielny-Bunde, V. Livina, S. Havlin, and A. Bunde, Physica A **330**, 240 (2003).

[32] P. Oświęcimka, J. Kwapień, and S. Drożdż, Phys. Rev. E **74**, 016103 (2006).

[33] A. Y. Schumann and J. W. Kantelhardt, Physica A **390**, 2637 (2011).

[34] J. Alvarez-Ramirez, E. Rodriguez, and J. C. Echeverría, Physica A **354**, 199 (2005).

[35] A. Bashan, R. Bartsch, J. W. Kantelhardt, and S. Havlin, Physica A **387**, 5080 (2008).

[36] E. Alessio, A. Carbone, and V. Castelli, G.and Frappietro, Eur. Phys. J. B **27**, 197 (2002).

[37] A. Carbone, G. Castelli, and H. E. Stanley, Phys. Rev. E **69**, 026105 (2004).

[38] G.-F. Gu and W.-X. Zhou, Phys. Rev. E **82**, 011136 (2010).

[39] P. A. Varotsos, N. V. Sarlis, E. S. Skordas, and M. S. Lazaridou, J. Appl. Phys. **103**, 014906 (2008).

[40] H. K. Tanaka, P. A. Varotsos, N. V. Sarlis, and E. S. Skordas, Proc. Jpn. Acad. Ser. B Phys. Biol. Sci. **80**, 283 (2004).

[41] P. A. Varotsos, N. V. Sarlis, H. K. Tanaka, and E. S. Skordas, Phys. Rev. E **72**, 041103 (2005).

[42] P. Varotsos, N. Sarlis, and E. Skordas, EPL **96**, 59002 (2011).

[43] P. Varotsos, N. Sarlis, and E. Skordas, EPL **99**, 59001 (2012).

[44] P. A. Varotsos, N. V. Sarlis, E. S. Skordas, and M. S. Lazaridou, Tectonophysics **589**, 116 (2013).

[45] N. V. Sarlis, E. S. Skordas, P. A. Varotsos, T. Nagao, M. Kamogawa, H. Tanaka, and S. Uyeda, Proc. Natl. Acad. Sci. USA **110**, 13734 (2013).

[46] N. V. Sarlis, E. S. Skordas, P. A. Varotsos, T. Nagao, M. Kamogawa, and S. Uyeda, Proc. Natl. Acad. Sci. USA **112**, 986 (2015).

[47] N. V. Sarlis, S.-R. G. Christopoulos, and E. S. Skordas, Chaos **25**, 063110 (2015).

[48] P. Varotsos, N. Sarlis, and E. Skordas, Acta Geophys. **64**, 841 (2016).

[49] P. A. Varotsos, N. V. Sarlis, E. S. Skordas, H. K. Tanaka, and M. S. Lazaridou, Phys. Rev. E **73**, 031114 (2006).

[50] P. A. Varotsos, N. V. Sarlis, E. S. Skordas, and M. S. Lazaridou, Appl. Phys. Lett. **91**, 064106 (2007).

[51] N. V. Sarlis, S.-R. G. Christopoulos, and M. M. Bemplidaki, EPL **109**, 18002 (2015).

[52] P. A. Varotsos, N. V. Sarlis, and E. S. Skordas, Phys. Rev. E **68**, 031106 (2003).

[53] P. A. Varotsos, N. V. Sarlis, E. S. Skordas, and M. S. Lazaridou, Phys. Rev. E **70**, 011106 (2004).

[54] C. K. Peng, S. Havlin, H. E. Stanley, and A. L. Goldberger, Chaos **5**, 82 (1995).

[55] T. C. Halsey, M. H. Jensen, L. P. Kadanoff, I. Procaccia, and B. I. Shraiman, Phys. Rev. A **33**, 1141 (1986).

[56] H.-O. Peitgen, H. Jurgens, and D. Saupe, Verlag, New York, NY (1992).

[57] B. B. Mandelbrot and J. W. van Ness, SIAM Rev. **10**, 422 (1968).

[58] M. Ausloos, N. Vandewalle, P. Boveroux, A. M. A., and K. Ivanova, Physica A **274**, 229 (1999).

[59] E. Frey and K. Kroy, Annalen der Physik **14**, 20 (2005).

[60] B. B. Mandelbrot and J. R. Wallis, Water Resources Research **5**, 321 (1969).

[61] J. Szulga and F. Molz, J. Stat. Phys. **104**, 1317 (2001).

[62] F. Schmitt, D. Schertzer, and S. Lovejoy, Applied stochastic models and data analysis **15**, 29 (1999).

[63] P. C. Ivanov, L. A. N. Amaral, A. L. Goldberger, S. Halvin, M. G. Rosenblum, H. E. Stanley, and Z. R. Struzik, Chaos **11**, 641 (2001).

[64] A. L. Goldberger, L. A. N. Amaral, J. M. Hausdorff, P. C. Ivanov, C.-K. Peng, and H. E. Stanley, Proc. Natl. Acad. Sci. USA **99**, 2466 (2002).

[65] K. Kotani, Z. R. Struzik, K. Takamasu, H. E. Stanley, and Y. Yamamoto, Phys. Rev. E **72**, 041904 (2005).

[66] I. Reyes-Ramírez and L. Guzmán-Vargas, EPL **89**, 38008 (2010).

[67] D. Makowiec, A. Rynkiewicz, J. Wdowczyk-Szulc, M. Zarczyńska-Buchowiecka, R. Galaska, and S. Kryszewski, Physiological Measurement **32**, 1681 (2011).

[68] A. L. Goldberger, L. A. N. Amaral, L. Glass, J. M. Hausdorff, P. C. Ivanov, R. G. Mark, J. E. Mictus, G. B. Moody, C.-K. Peng, and H. E. Stanley, Circulation **101**, E215 (see also `www.physionet.org`) (2000).

[69] D. S. Baim, W. S. Colucci, E. S. Monrad, H. S. Smith, R. F. Wright, A. Lanoue, D. F. Gauthier, B. J. Ransil, W. Grossman, and E. Braunwald, J. Am. Coll. Cardiol. **7**, 661 (1986).

[70] G. B. Moody, computer code `ann2rr` available from `http://www.physionet.org/physiotools/wag/ann2rr-1.htm`.

[71] Y. Ashkenazy, P. C. Ivanov, S. Havlin, C. K. Peng, Y. Yamamoto, A. L. Goldberger, and H. E. Stanley, Comput. Cardiol. **27**, 139 (2000).

[72] Y. Ashkenazy, P. C. Ivanov, S. Havlin, C.-K. Peng, A. L. Goldberger, and H. E. Stanley, Phys. Rev. Lett. **86**, 1900 (2001).

[73] L. A. N. Amaral, P. C. Ivanov, N. Aoyagi, I. Hidaka, T. Tomono, A. L. Goldberger, H. E. Stanley, and Y. Yamamoto, Phys. Rev. Lett. **86**, 6026 (2001).

[74] A. L. Goldberger, L. A. N. Amaral, J. M. Hausdorff, P. C. Ivanov, C.-K. Peng, and H. E. Stanley, Proc. Natl. Acad. Sci. USA **99**, 2466 (2002).

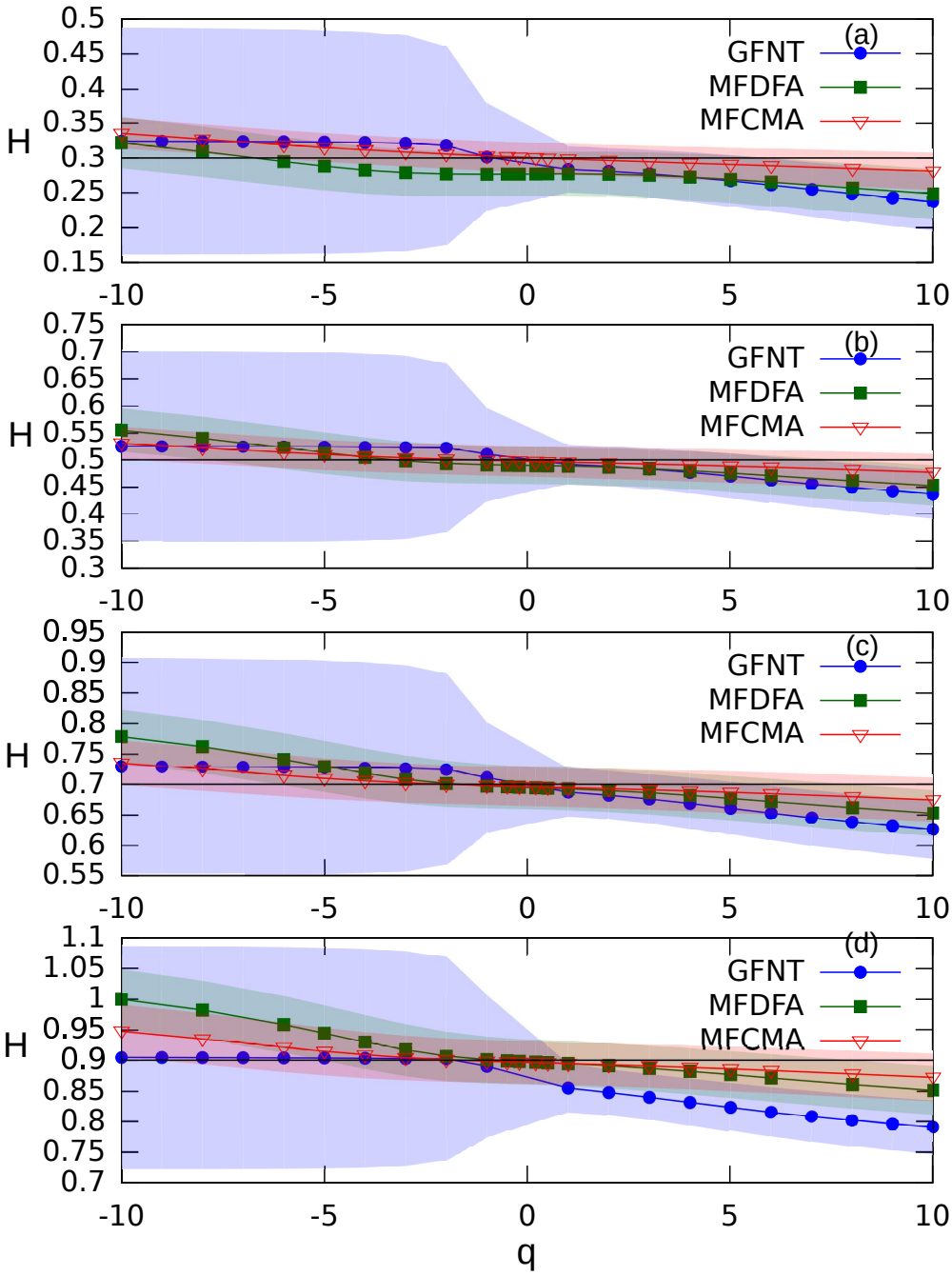

FIG. 1: The average generalized scaling exponent estimated from $\chi_H(q)$ of GFNT (blue color) and $h(q)-1$ of MFDFA (green color) versus q as it results (see subsection III A) from 3×10^2 fBm time series with $H=0.3$, $H=0.5$, $H=0.7$, and $H=0.9$ (cf. these theoretical values are indicated by the black horizontal lines). The red inverted triangles correspond to the results obtained when using MFCMA. The colored regions refer to $\pm$ one standard deviation.

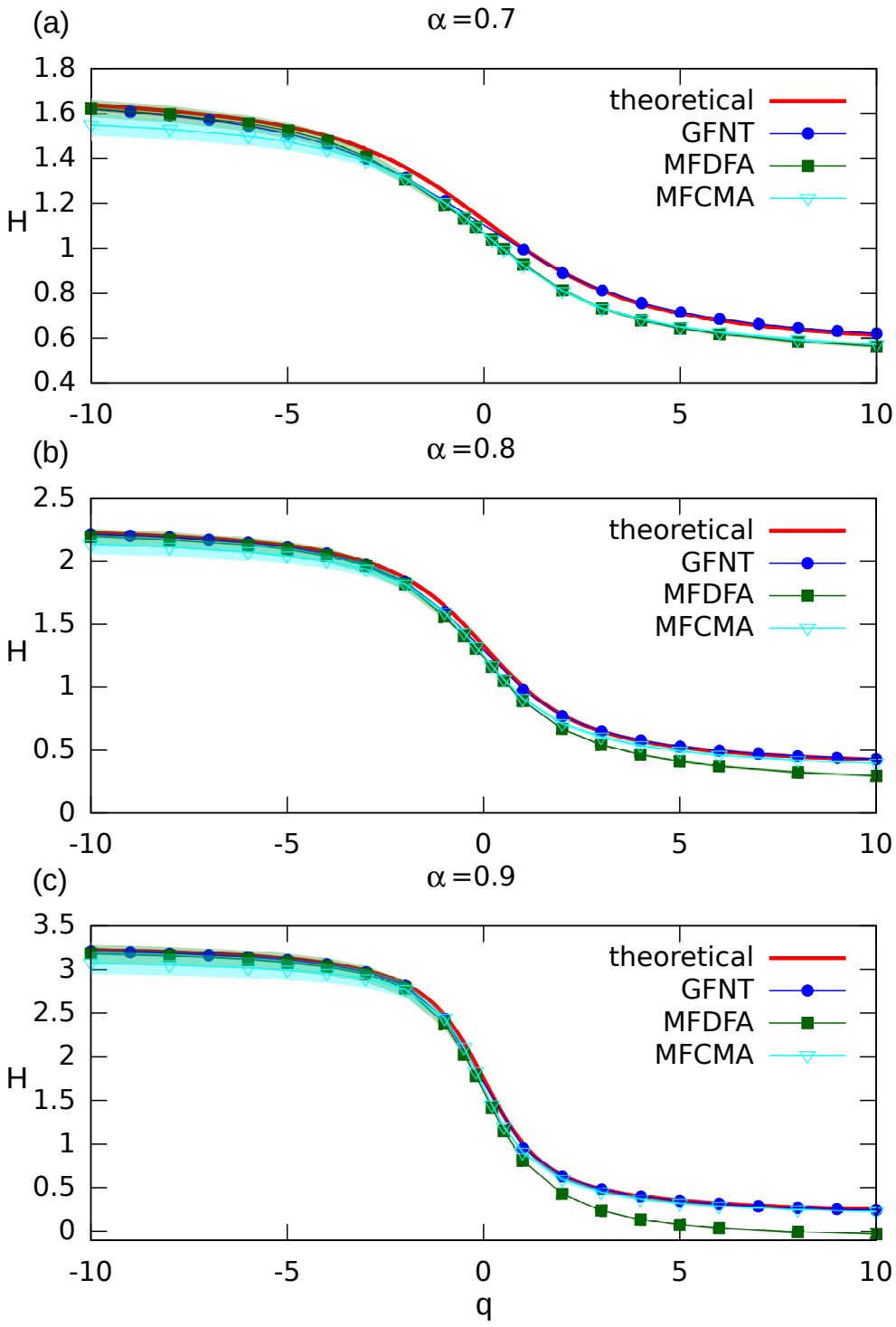

FIG. 2: The generalized scaling exponents $h(q)$ calculated by MFDFA (green color) and $\chi_H(q)$ by GFNT (blue color) versus the theoretical set (red line) of generalized scaling exponents $h(q)$ for binomial multifractal time series with $\alpha = 0.7$ (a), 0.8 (b), and 0.9 (c). The cyan inverted triangles correspond to the results obtained when using MFCMA. The colored regions indicate the estimation error.

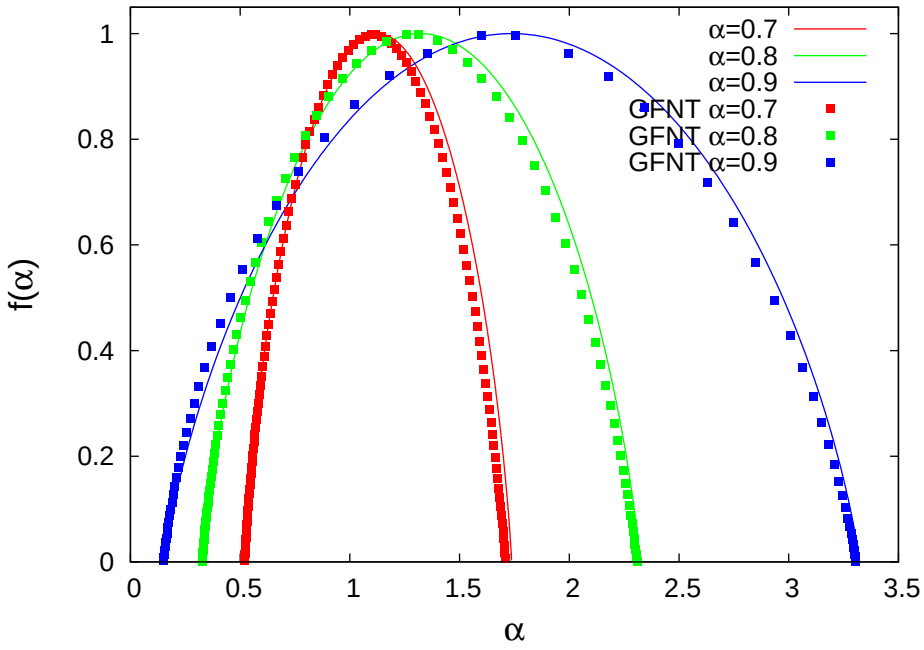

FIG. 3: Singularity spectra $f(\alpha)$ versus exponent α for the binomial multifractal time series with $\alpha = 0.7$ (red), 0.8 (green), and 0.9 (blue). In each case, the theoretical spectrum estimated using Eq.(19) is depicted with the solid curve in each case, while that calculated on the basis of the exponents $\chi_H(q)$, with a step of $\delta q = 0.1$, of GFNT is shown with the solid squares.

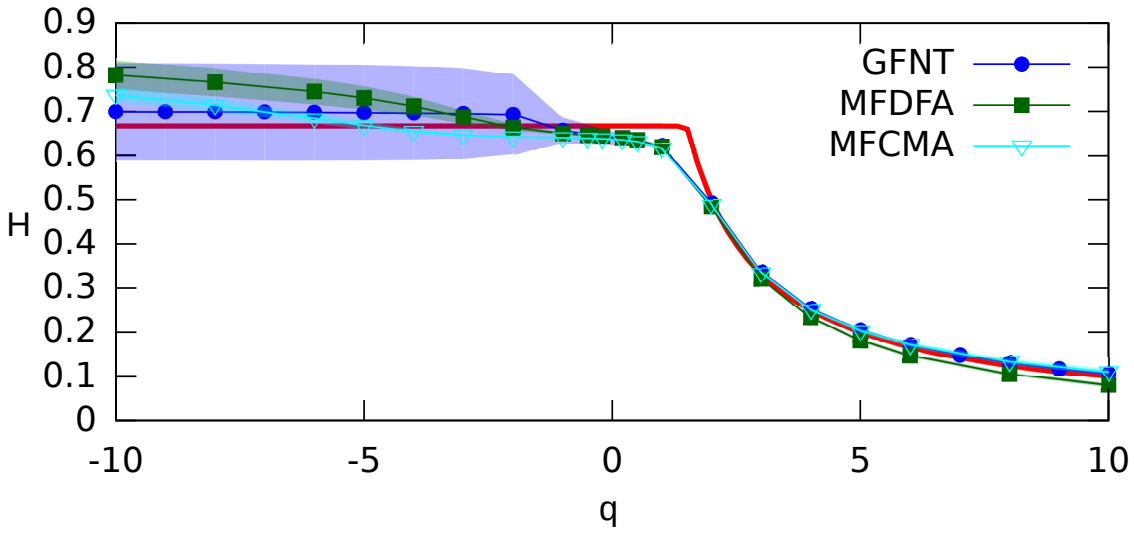

FIG. 4: The generalized scaling exponents $h(q)$ calculated by MFDFA (green color) and $\chi_H(q)$ by GFNT (blue color) versus the theoretical set of generalized scaling exponents $h(q)$ for a Lévy stable process with $\alpha_L = 1.5$ (red thick line). The cyan inverted triangles correspond to the results obtained when using MFCMA. The colored regions indicate the estimation error.

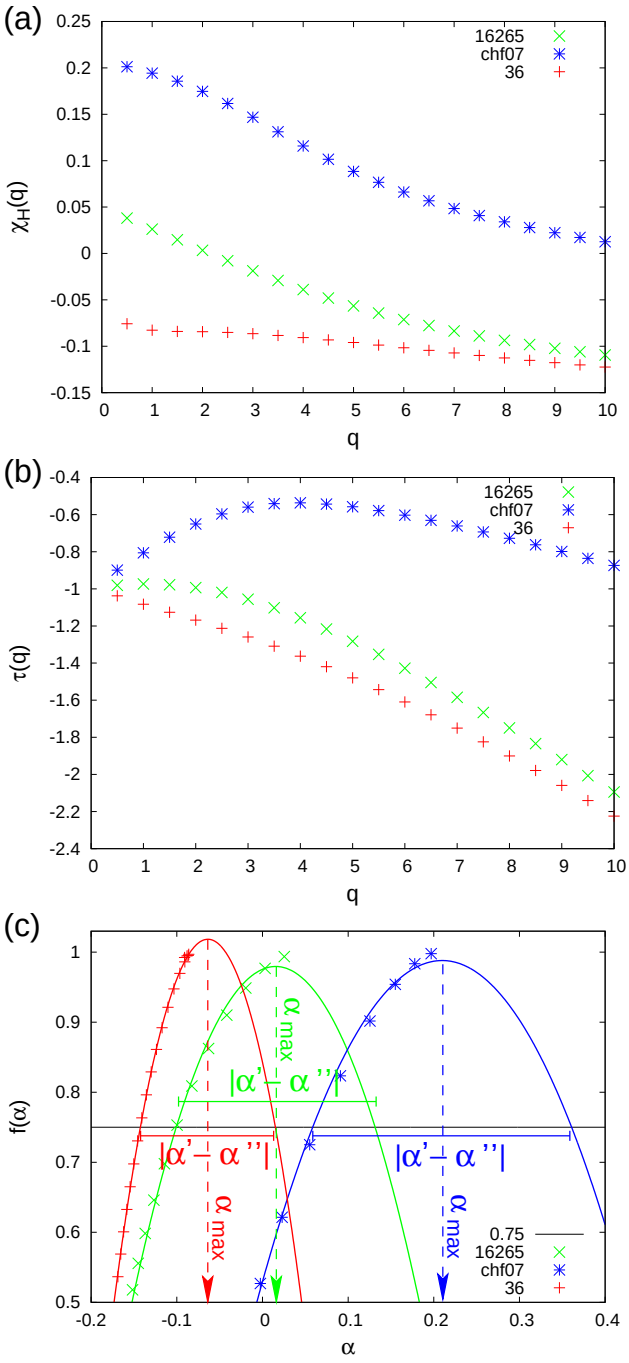

FIG. 5: The values of $\chi_H(q)$ estimated from GFNT for scales l in the range 5 to $\approx N/4$, where N is the number of heartbeats available in each record, are depicted in (a). These values are firstly converted to $\tau(q)$ through Eq.(15) as shown in (b) and then a three-point differentiation leads to the singularity spectrum depicted in (c). Examples of a healthy individual, labeled '16265', a congestive heart failure subject, labeled 'chf07', and a sudden cardiac death individual, labeled '36' are included in these panels. In (c), the estimation of the quantities α_{max} and $|\alpha' - \alpha''|$ based on a parabolic fit is also shown.

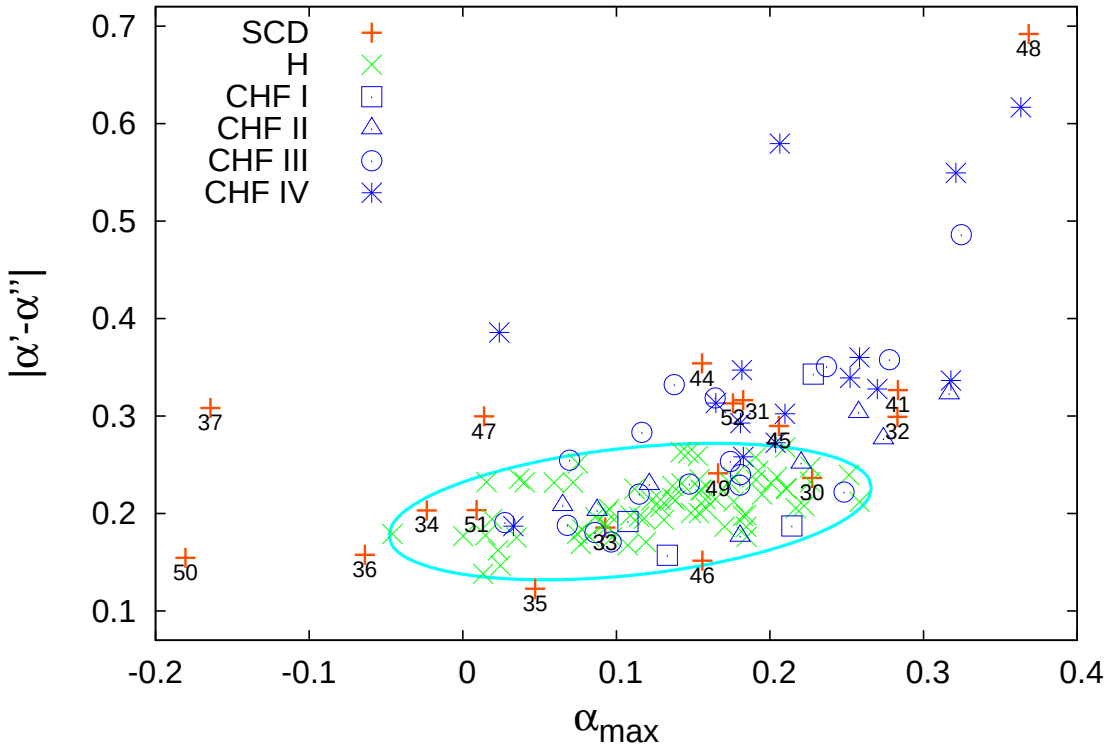

FIG. 6: The values of $|\alpha' - \alpha''|$ versus α_{max} for the 134 NN time series analyzed. The red pluses correspond to the values estimated for the 18 individuals of the sudden cardiac death (SCD) database, the green crosses to the 72 healthy and the four different blue symbols to the four different (indicated by roman numerals) NYHA class patients suffering from congestive heart failure (CHF). The cyan ellipse, that has been drawn as a guide to the eye, encloses all the points corresponding to healthy individuals. The numbers indicate the record ID for each SCD individual.